Journal of Molecular Modeling (2022) 28:406
https://doi.org/10.1007/s00894-022-05393-4

ORIGINAL PAPER

Comprehensive theoretical study on safety performance and mechanical properties of 3-nitro-1,2,4-triazol-5-one (NTO)–based polymer-bonded explosives (PBXs) via molecular dynamics simulation

Ying Huang[1] · Ruijun Gou[1] · Shuhai Zhang[1] · Xiaofeng Yuan[1] · Yahong Chen[1]

Received: 2 September 2022 / Accepted: 15 November 2022 / Published online: 1 December 2022

Abstract

3-nitro-1,2,4-triazol-5-one (NTO)–based polymer-bonded explosives (PBXs) have been widely used in insensitive munitions, but the main properties of NTO-based PBXs such as compatibility, safety performance, and mechanical properties are rarely reported. In this work, molecular dynamics simulation was carried out to study interface interactions of NTO-based PBXs, in which hydroxy-terminated polybutadiene (HTPB), ethylene–vinyl acetate copolymer (EVA), glycidyl azide polymer (GAP), poly-3-nitratomethyl-3-methyl oxetane (Poly-NIMMO), and ester urethane (Estane5703) are selected as binders. The binding energy analysis indicates that the order of compatibility is NTO/GAP > NTO/Estane5703 > NTO/HTPB > NTO/Poly-NIMMO > NTO/EVA. Radial distribution function analysis results show that the interface interaction is mainly the hydrogen bond between H atoms of NTO and O atoms of Estane5703, HTPB, EVA, and Poly-NIMMO or N atoms of GAP. The values of cohesive energy density verify that the safety is NTO/GAP > NTO/Poly-NIMMO > NTO/HTPB > NTO/EVA > NTO/Estane5703. Mechanical properties results show that GAP and EVA would improve the plasticity of the systems effectively. Furthermore, it can be found that the most favorable interactions occur between the NTO (1 0 0) crystal face and binders.

Keywords NTO · Molecular dynamics simulation · Polymer-bonded explosives (PBXs) · Interfacial interaction · Mechanical properties; Safety performance

Introduction

The composite explosive made up of energetic components and additives in proper proportion meets various requirements of weapons and ammunition, and is the main form of energetic materials used in weapon systems [1]. With the development of polymer materials, polymer-bonded explosives (PBXs) are commonly used in the field of military because of its high energy density, good safety performance, and mechanical properties [2–4]. Owing to the influence of the polymer binder and functional additives, the investigations of polymer-bonded explosives mainly focus on compatibility, safety performance, and mechanical properties. Due to the crucial role of these characteristics in the design, manufacture, transportation, storage, and usage of PBXs, it is necessary to analyze the compatibility, mechanical properties, and safety performance between the binder and explosive molecules in PBXs.

Researchers have done some reports on the interface interactions of PBXs [5–11]. Xiao et al. [12] compared and analyzed the mechanical properties of the interface models composed of different crystal faces of 1,3,5-triamino-2,4,6-trinitrobenzene (TATB) and typical fluorine-containing binder, and found that the effectiveness of different crystal faces in improving mechanical properties was (0 1 0) ≈ (1 0 0) > (0 0 1). Lu et al. [13] simulated PBXs composed of hexanitrohexaazaisowurtzitane (CL-20) and glycidyl azide polymer (GAP) with different groups, and the results showed that the addition of the binder could improve the ductility and impact resistance of PBXs. Furthermore, it can be found that the addition of a binder will reduce the sensitivity of PBX systems. Xu et al. [14] conducted molecular dynamics simulation analysis by constructing the interface models composed of ε-CL-20 and polyurethane (Estane5703), GAP, hydroxy-terminated polybutadiene (HTPB), polyethylene glycol (PEG), and copolymers polymerized from

✉ Ruijun Gou
grjzsh@163.com

[1] School of Environment and Safety Engineering, North University of China, Taiyuan 030051, Shanxi, China

vinylidenedifluoride and chlorotrifluoroethylene with the molar ratios of 1:4 (F_{2314}). Through comparing the binding energy, heat capacity, mechanical properties, and energy characteristics, the four binders except F_{2314} are good choices. Therefore, the addition of binder can improve the mechanical properties of PBXs, and can also significantly decrease the sensitivity characteristics of PBXs and improve its safety. As a typical high energy density material (HEDM), 3-nitro-1,2,4-triazol-5-one (NTO) [15] is widely used in the design of novel formulations because of its excellent performance. The density of NTO is as high as 1.93 g•cm^{-3} [16]. Its detonation velocity is 8200 m•s^{-1}, which is higher than the TATB explosive [17]. And the safety performance is far superior to HMX and RDX explosives. In addition, the synthetic process of NTO is simple and the cost is low [18]. Researchers have done extensive and in-depth research on the performance of NTO-based PBXs [19, 20]. Moreover, Zhou et al. [21] measured the contact angles of NTO, GAP, HTPB, and polyurethane by using a DCAT21 dynamic contact angle/surface tension meter, and then calculated the surface free energy, adhesive work, and spreading coefficient. The data demonstrate that all three binders selected can produce excellent wettability and coating performance on the surface of the NTO explosive. We compare the adhesive work to obtain the order of interactions being NTO/GAP > NTO/polyurethane > NTO/HTPB.

Although the formulations of NTO-based PBXs have been broadly used in all kinds of insensitive munitions (IMs), there are few reports on the mechanical properties and safety performance of NTO-based PBXs [22–24]. With the increasing requirements of performance of NTO-based PBXs in the complex battlefield environment, it is urgent to study the safety performance and mechanical properties of NTO and binders. The interface model [25–29] established by using computer simulation technology to cleave the explosive has been widely used to study and predict the performance of PBXs, which can effectively solve the problems of experimental safety and time-consuming, and can consider many influencing factors to accurately predict the performance of PBX formulation. Therefore, in this paper, the molecular dynamics simulation of NTO models and five composite systems such as NTO/HTPB and NTO/GAP was carried out, and the interface interactions, cohesive energy density, mechanical properties, and other related parameters were calculated. The performance parameters of pure NTO systems and NTO-based PBX composite systems were compared, and the differences in PBX performance under different factors such as separate binders and different crystal faces were studied. The microscopic theory of the interaction between binders and NTO was obtained by calculation, and the sensitivity and mechanical properties of different PBXs were predicted, which provided theoretical guidance for the design and research of NTO-based PBX formulations.

Simulation details

Choice of force field

One of the decisive factors for the dependability of molecular dynamics simulation results is the selection of an appropriate force field. Condensed-phase optimized molecular potentials for atomic simulation studies (COMPASS) force field [30] is selected during the simulation of the NTO and binder interface models. COMPASS is based on experimental data and adopts a mixed method consisting of ab initio and empirical methods to obtain the parameters of various bonds in molecules, and then debug the force field parameters. Considering the effects of van der Waals' non-bonding parameters, the condensed-phase-optimized force field is generated. Subsequently, before simulating the CL-20/NTO composite system, Hang et al. [31] concluded that the COMPASS force field is more suitable for NTO crystal by comparing the NTO lattice parameters obtained under different force fields with the experimental results. In addition, the COMPASS force field has been applied to analyze the related properties of PBXs composed of HTPB [9, 32], ethylene–vinyl acetate copolymer (EVA) [33], GAP [34], poly-3-nitratomethyl-3-methyl oxetane (Poly-NIMMO) [35], and Estane5703[36, 37].

The NTO crystal structure was obtained from Cambridge Crystallographic Data Centre [38] (CCDC: 166,510) and is shown in Fig. 1. The initial crystal cell consists of four NTO molecules (molecular formula: $C_2H_2O_3N_4$), which belongs to the P21/c (14) space group. The NTO crystal cell was expanded by 4 × 4 × 4, and the stable configuration was obtained by optimization and NPT simulation under the COMPASS force field. The parameter comparison is shown in Table 1. It can be seen from Table 1 that the error of the lattice parameters of the supercell is less than 3.5% within the acceptable error range, which indicates the chosen force field can precisely represent the properties of the systems. Therefore, the COMPASS force field is selected for molecular dynamics simulation.

Selection of crystal face

The molecular mechanics (MM) optimization of the NTO initial crystal cell was carried out under the force field of COMPASS. MM optimization is to make the molecule adjust its geometric shape so that its bond length and bond angle are as close to the natural values as possible, and at the same time, to make the non-bond interaction in the minimum state. And the optimization algorithm used in the calculation process is "Smart," the maximum number

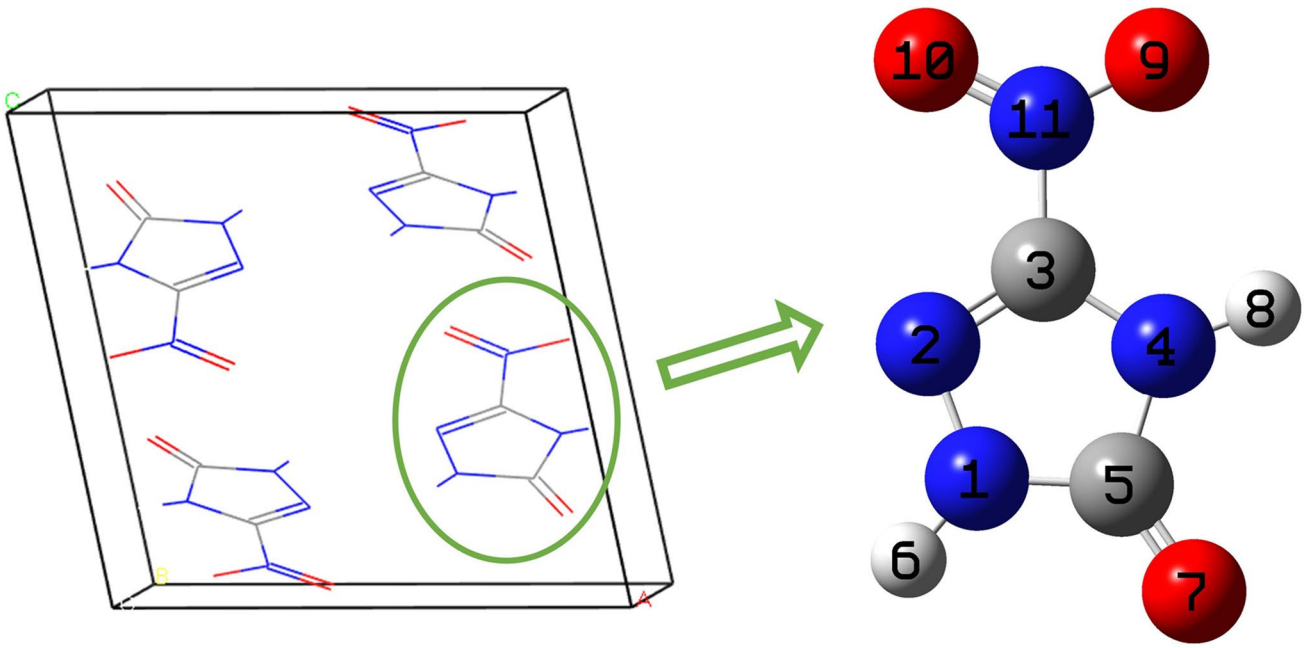

Fig. 1 Crystal structure and molecular structure of NTO

Table 1 Comparison of NTO crystal cell parameters and errors

Lattice parameter	*a*/Å	*b*/Å	*c*/Å	*β*/°	*α* = *γ*/°
Experiment	9.3255	5.4503	9.04	101.474	90
COMPASS	9.639	5.633	9.344	101.474	90
Relative error/%	3.362	3.352	3.363	0.000	0.000

Table 2 Morphologically important faces of NTO crystal

h k l	Surface area/Å^2	Total facet area/%
1 0 0	66.55	37.36
1 0 − 2	78.06	24.57
1 1 − 1	82.26	17.62
0 1 1	87.36	16.34

of iterations is 50,000 steps, and the accuracy is "Fine." Atom-based and Ewald's summation methods are used to calculate van der Waals' interaction and electrostatic interaction, respectively. The growth morphology calculation of the optimized structure shows that the important crystal faces of NTO crystal morphology are (1 0 0), (1 0 − 2), (1 1 − 1), and (0 1 1), respectively, as shown in Table 2. These four crystal faces are the relatively stable four crystal faces in NTO crystal morphology, which means that binders have a higher probability of contacting with these four crystal faces. Therefore, these four crystal faces are selected for simulation calculation.

Construction of the model

The NTO crystal cell was cleaved along the (1 0 0), (1 0 − 2), (1 1 − 1), and (0 1 1) crystal faces with four molecular layer thicknesses. Add repeating units in the directions *a* and *b* of structure to the tangent plane, so that the supercell contains 256 NTO molecules. The periodic structure is established to obtain the model for calculation.

We construct the molecular model of the high polymer according to the polymer structure of each binder. And the specific information such as density, chain number, and total atom number of the five binders are listed in Table 3. All repeating units are connected head to tail, and the terminal groups are saturated with CH_3, H, and OH respectively as appropriate. We optimize the constructed

Table 3 The details of the five polymer models

	HTPB	GAP	EVA	Poly-NIMMO	Estane5703
Chain numbers	6	6	5	4	2
Density/g•cm^{-3}	0.908	1.27	0.95	1.46	1.25
The total number of atoms	324	234	370	240	334

polymer chains to obtain stable configurations with minimum energy, as shown in Fig. 2.

The interface models (NTO/HTPB, NTO/EVA, NTO/GAP, NTO/Poly-NIMMO, and NTO/Estane5703 systems) were constructed. The required number of polymer chains is determined according to the proportion of binder (the mass ratio is about 5%) [39]. The contents of HTPB, EVA, GAP, Poly-NIMMO, and Estane5703 are 5.2%, 5.6%, 5.4%, 5.2%, and 6.4% respectively. According to the calculated number of polymer chains and the theoretical density, the optimized polymer chain is constructed into an amorphous unit cell, which makes it present a real state. In which *a* and *b* correspond to the crystal face parameters of NTO. The periodic structures of five binders were respectively compounded on the NTO crystal models, and 20 composite models were obtained. The composite model is compressed in the *c* direction, and MM optimization is performed after each compression until it approaches the calculated theoretical density. The theoretical density is the maximum limit of density that the composite system of NTO and binder can reach under general conditions. And it can be calculated according to Eq. (1).

$$\rho_{max}=\frac{\sum g_i}{\sum\left(\frac{g_i}{\rho_i}\right)} \tag{1}$$

where ρ_{max} represents the maximum limit density of mixed explosives, g_i represents the mass fraction of substance *i*, and ρ_i represents the theoretical density of substance *i*. The final optimized configuration is treated as the initial configuration of molecular dynamics simulation. The main modeling process is shown in Fig. 3, taking the construction of the NTO (1 0 0)/HTPB system as an example.

Molecular dynamics (MD) simulation

MD simulation was carried out on the optimized NTO models and the optimized interface models of NTO/HTPB, NTO/EVA, NTO/GAP, NTO/Poly-NIMMO, and NTO/Estane5703 under the COMPASS force field. The simulated environment of MD is 298 K, and the binding energy, cohesive energy density, and radial distribution function are analyzed by isothermal-isochoric (NVT) ensemble. In addition, the mechanical properties are simulated and analyzed by an isothermal-isobaric (NPT) ensemble. Andersen's thermostat method [40] is used in the calculation process, and atom-based and Ewald's addition methods [41] are used for the calculation of van der Waals' action and electrostatic action, with the cutoff distance of 15.5 Å and the time step of 1 fs. In the NPT simulation process, the pressure control mode is set to Berendsen for 300 ps to

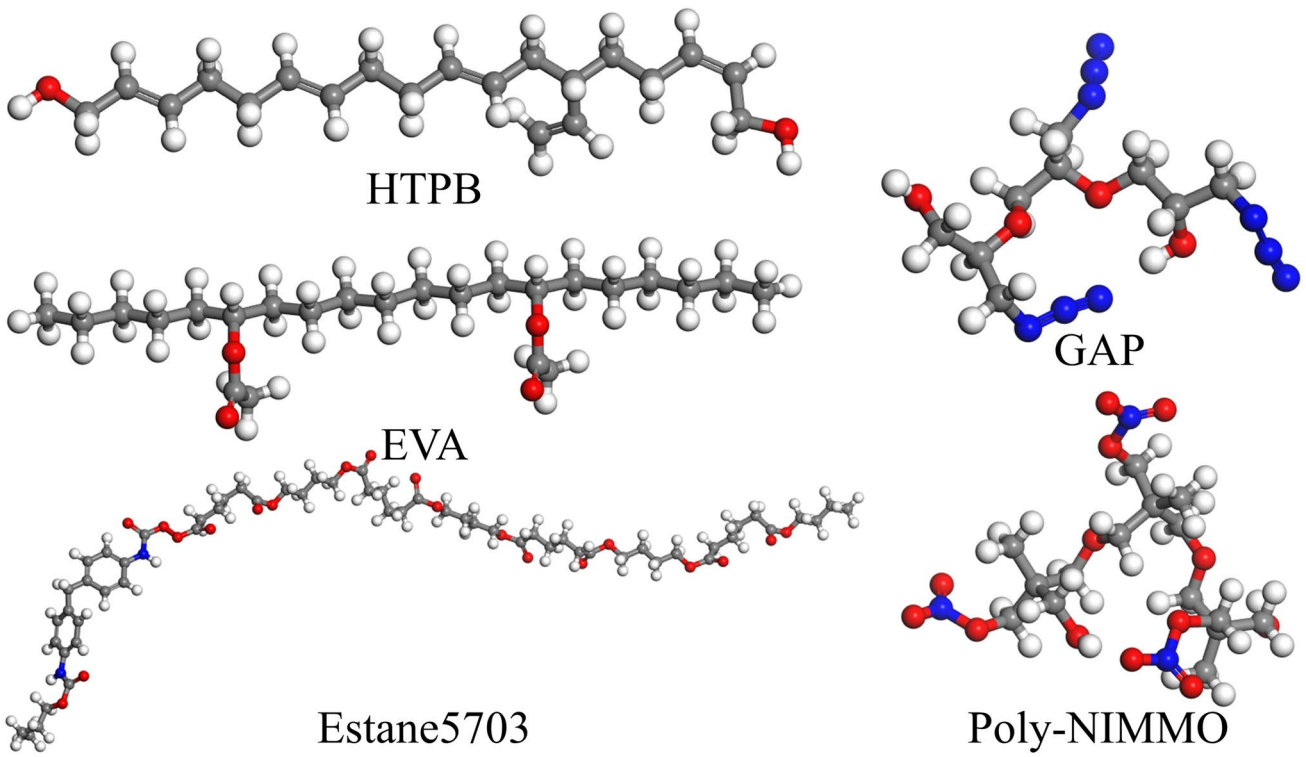

Fig. 2 The stable configurations of polymer binders

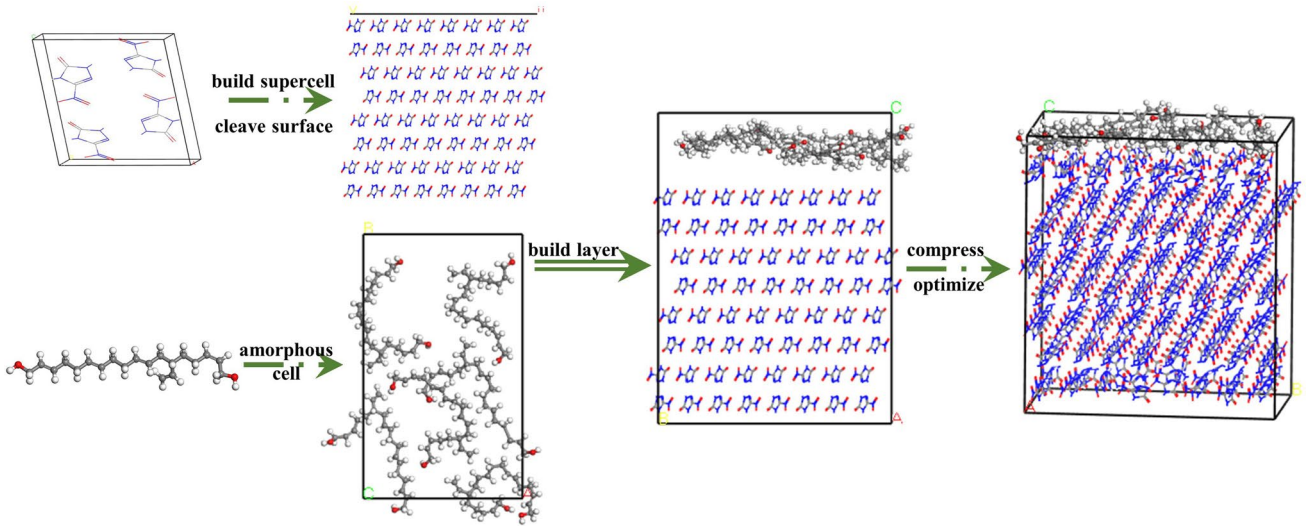

Fig. 3 The procedure of model establishment of the NTO (1 0 0)/HTPB system

eliminate the irrationality of the structure, and then set to Parrinello-Rahman [42] for 200 ps to obtain relevant statistical data. Then, the NVT-MD simulation of each model lasts for 300 ps. Based on the above set environmental conditions, all models are simulated by molecular dynamics to ensure the convergence and stability of the simulated energy and temperature curves, so as to obtain a stable simulation structure. The trajectory file outputs one frame every 500 steps, and the last 200 frames are selected for analysis.

Results and discussion

Equilibrium of the system

In order to accurately calculate the binding energy and mechanical properties and other related properties of systems, the systems used for statistical analysis should reach equilibrium. The criterion of equilibrium is determined by both temperature and energy; that is, their curves fluctuate between 5 and 10% [43]. Take the curves of energy and temperature of NTO (1 0 0)/HTPB composite system NVT simulation as an example, as shown in Fig. 4. It can be found that in the equilibrium interval of MD simulation, the temperature amplitude and energy fluctuation of the last 100 ps are all less than 5%, indicating that the system has reached equilibrium. Similarly, the NTO models and NTO-based PBX interface models have reached equilibrium after MD simulation.

Binding energy

Binding energy (E_{bind}) is a good indicator of the interaction between NTO and polymer binder, which is also a very significant quantity to assess the physical compatibility between explosive crystal and polymer binder. The larger the binding energy, the stronger the interaction between them, that is, the better the compatibility between explosive molecules and polymers [12]. The binding energy is defined as the negative value of the interaction energy of the system. The equation used is as follows:

$$E_{bind} = -E_{int} = E_{total} - E_{NTO} - E_{polymer} \tag{2}$$

where E_{bind} is the binding energy of NTO and binder, E_{int} is the interaction energy, E_{total} is the total energy of the equilibrium structure of the composite system, E_{NTO} is the energy of only NTO in the composite system after the binder is removed, and $E_{polymer}$ is the energy of only the binder in the composite system after the NTO molecules are removed.

The last 200 frames of the trajectory file are analyzed by Perl script; the final result is the average of all binding energies. We calculate the binding energy per unit area $E_{bind}{}'$ and the average binding energy E_{ave} to comprehensively consider the influence of each crystal face. $E_{bind}{}'$ and E_{ave} [32] can be calculated as the following equations.

$$E_{bind}{}' = \frac{E_{bind}}{S} \tag{3}$$

$$E_{ave} = \sum E_{\mathrm{bind}}{}' \cdot \%S \tag{4}$$

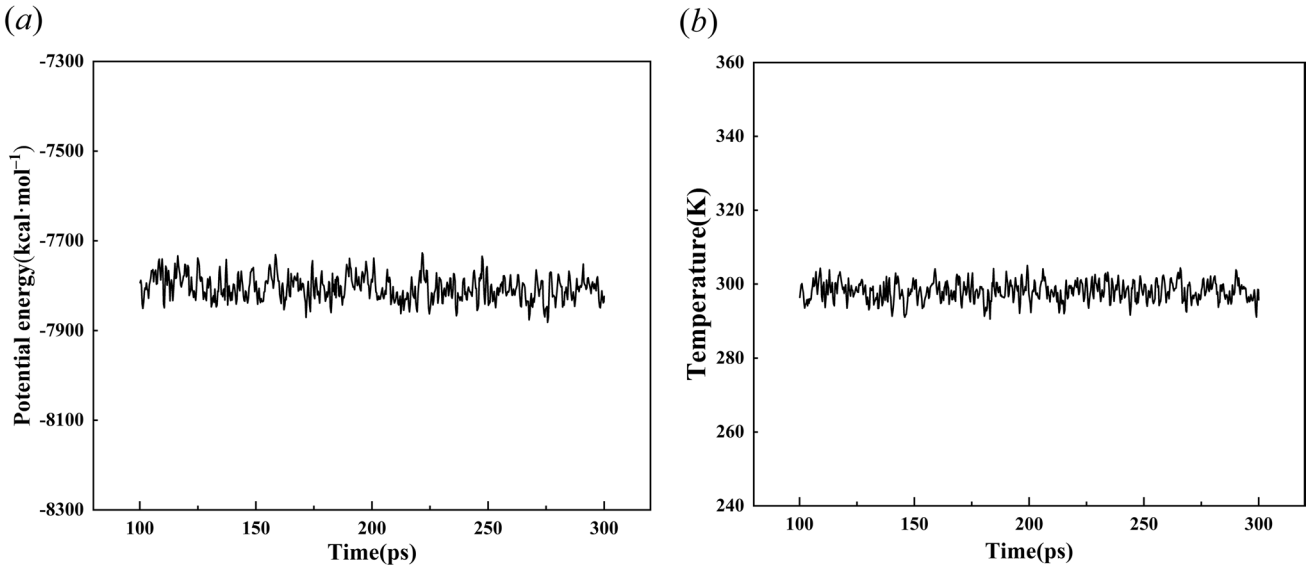

Fig. 4 Fluctuation curves of energy (**a**) and temperature (**b**) of NTO (1 0 0)/HTPB composite system

Table 4 The binding energies (E_{bind}/kJ·mol^{-1}), the binding energies per unit area (E_{bind}'/kJ·mol^{-1}·Å^{-2}), and the average binding energies (E_{ave}/kJ·mol^{-1}·Å^{-2}) between NTO and five binders

Systems	Facet	E_{total}	E_{NTO}	E_{binder}	E_{bind}	E_{bind}'	E_{ave}
NTO/HTPB	1 0 0	− 7796.58	− 7474.43	87.42	409.56	6.15	5.42
	1 0 − 2	− 7214.85	− 6909.80	134.33	439.38	5.63	
	1 1 − 1	− 7318.90	− 7011.86	134.20	441.24	5.36	
	0 1 1	− 7226.79	− 6928.66	124.49	422.61	4.84	
NTO/GAP	1 0 0	− 7675.21	− 7460.29	269.05	483.97	7.27	5.89
	1 0 − 2	− 7086.58	− 6929.46	292.01	449.12	5.75	
	1 1 − 1	− 7220.75	− 7048.49	276.35	448.61	5.45	
	0 1 1	− 7098.28	− 6953.82	282.35	426.81	4.89	
NTO/Estane5703	1 0 0	− 6195.17	− 7480.78	1725.24	439.63	6.61	5.70
	1 0 − 2	− 7446.65	− 6864.66	− 162.43	419.57	5.37	
	1 1 − 1	− 7614.25	− 6989.22	− 148.82	476.21	5.79	
	0 1 1	− 7618.34	− 6992.34	− 147.22	478.77	5.48	
NTO/EVA	1 0 0	− 8015.79	− 7498.21	− 158.58	358.99	5.39	4.52
	1 0 − 2	− 7452.03	− 6978.69	− 137.54	335.80	4.30	
	1 1 − 1	− 7596.59	− 7088.63	− 129.62	378.35	4.60	
	0 1 1	− 7470.10	− 6999.76	− 130.39	339.94	3.89	
NTO/Poly-NIMMO	1 0 0	− 7867.85	− 7530.14	49.04	386.75	5.81	4.78
	1 0 − 2	− 7290.85	− 6961.45	33.23	362.64	4.65	
	1 1 − 1	− 7405.15	− 7082.42	38.35	361.08	4.39	
	0 1 1	− 7295.96	− 6968.44	41.37	368.90	4.22	

It can be seen from Table 4 that the binding energies between different binders and NTO are positive, demonstrating that these systems can exist stably. The unit binding energies of all crystal faces are shown in Fig. 5. For HTPB, GAP, and Poly-NIMMO, their compatibilities with different crystal faces of NTO are accordant; that is, the descending order of binding energies is (1 0 0) > (1 0 − 2) > (1 1 − 1) > (0 1 1). However, the interface interactions between NTO/Estane5703 and NTO/EVA composite systems are different from them. The (1 0 0) crystal face still has the maximum binding energy, but the (1 1 − 1) crystal face is the second. Generally speaking, the (1 0 0) surface has the strongest interaction with five polymers. That is to say, the polymer binders used in this study tend to concentrate and interact with the NTO (1 0 0) surface.

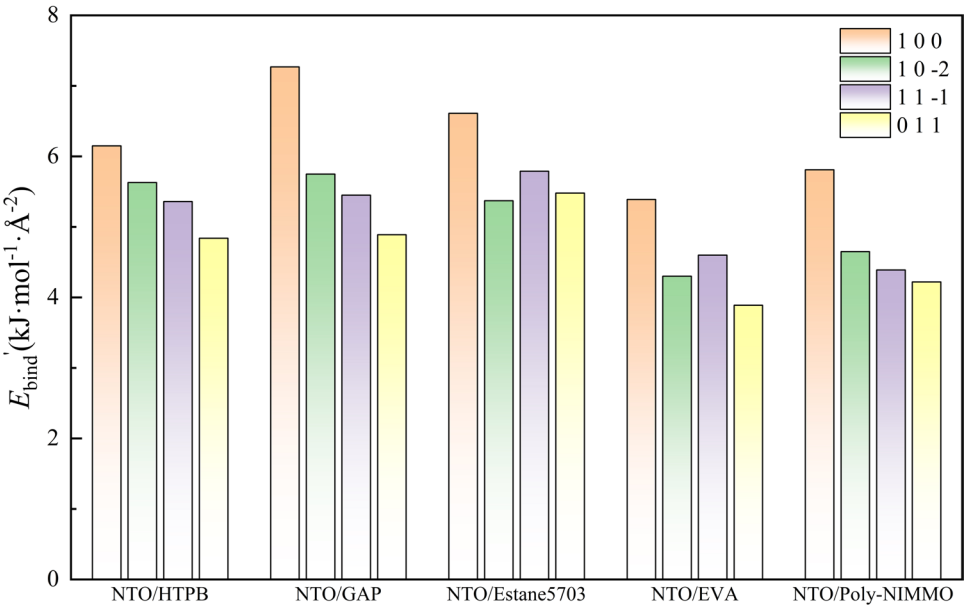

Fig. 5 Average binding energy E_{bind}' of different crystal faces of NTO-based PBXs

Furthermore, it can be found that the binding energies between (1 0 0) and (1 0 − 2) crystal faces and GAP are the largest, and that between (1 1 − 1) and (0 1 1) crystal faces and Estane5703 are the strongest. This data shows that (1 0 0) and (1 0 − 2) crystal faces have the strongest interactions with GAP, while (1 1 − 1) and (0 1 1) crystal faces have the best compatibilities with Estane5703. At the same time, for all crystal faces, the binding energies of Poly-NIMMO and EVA with different crystal faces are ranked last. This situation manifests that PBXs containing Poly-NIMMO and EVA may have poor compatibility.

According to the above analysis, we can predict that the compatibility order is NTO/GAP > NTO/Estane5703 > NTO/HTPB > NTO/Poly-NIMMO > NTO/EVA. Then, we make a comprehensive analysis by comparing the average binding energy. Comparing the five binders selected in this study, we can observe that the NTO/GAP systems have higher average binding energy. This means that GAP has the best compatibility among the five binders. The order of average binding energy is NTO/GAP > NTO/Estane5703 > NTO/HTPB > NTO/Poly-NIMMO > NTO/EVA. It is readily noted that the result is consistent with the above-mentioned predicted result. Furthermore, the order of binding energies among NTO/GAP, NTO/Estane5703, and NTO/HTPB models is consistent with the results obtained by Zhou et al. [21] by measuring the contact angles of NTO, GAP, HTPB, and polyurethane with DCAT21 dynamic contact angle/surface tensiometer. It proves the correctness of this work.

Radial distribution function

The binding energy analysis proves that there are interactions between PBX interfaces. The radial distribution function (RDF) of the composite system was analyzed to further discuss the interaction between the binder and NTO. RDF is the ratio of local density to bulk density of the system, which describes how the density varies with the distance from the referenced particle. The local density near the referenced atom is distinct from the bulk density of the system, but the bulk density far from the referenced atom is the same as the local density. That is, when the value of r is large, the value of $g(r)$ is approximated to 1. According to the meaning of RDF, its equation [44] is defined as:

$$g(r)=\frac{dN}{\rho 4\pi r^2 dr} \tag{5}$$

where r is the atomic spacing, ρ is the atomic density, and $g(r)$ represents the probability of the atom to be analyzed appearing at the specified distance r from the reference atom. The type of interaction can be judged according to the peak position of $g(r)$, and the magnitude of the interaction can be inferred from the sequence of the peak position. What is worth mentioning is the acidity of NTO. Hu et al. [45] used density functional theory to analyze the intermolecular interaction between NTO and 2,6-diamino-3,5-dinitropyrazine-1-oxide (LLM-105) to consider the acidity of NTO. We can speculate that the hydrogen bond formed with the H atoms of NTO can fix the active H atoms of NTO, and then stabilize the system. Therefore, we choose to analyze the radial distribution function of the atomic pair composed of the H atoms of NTO and the N atoms or O atoms of the binder.

Generally speaking, intermolecular interactions [35] include hydrogen bond interaction (2.6–3.1 Å), van der Waals' interaction (3.1–5.0 Å), and Coulomb's interaction

(> 5.0 Å). The purpose of RDF analysis of PBXs is to find out the peak of $g(r)$ in the same interval of r and the sequence of its appearance, so as to get the types and strengths of the interactions between different binders and explosive molecules. Through RDF analysis of O atoms or N atoms in polymers and H atoms in NTO, the interaction types and strengths of NTO-based PBXs were obtained.

Figure 6 shows the RDF between the H atoms of NTO and O atoms of five binders. It can be clearly seen from Fig. 6 that the systems with different crystal faces have an obvious main peak in the range of 2.6–3.1 Å, which proves that the interface interaction of each PBX system is mainly hydrogen bond interaction. There is also a peak value in the range of 3.1–5.0 Å, indicating that there is van der Waals'

Table 5 The peak points and peak values of hydrogen bond interaction between H atoms of NTO and O atoms of binders

Systems	Facet	1 0 0	1 0 −2	1 1 −1	0 1 1
NTO/HTPB	*r*/Å	2.61	2.65	3.09	2.85
	g(*r*)	0.45	0.47	0.67	0.69
NTO/GAP	*r*/Å	2.61	2.67	2.63	2.65
	g(*r*)	0.43	0.33	0.42	0.44
NTO/Estane5703	*r*/Å	2.65	2.95	2.81	2.91
	g(*r*)	0.43	0.34	0.36	0.42
NTO/EVA	*r*/Å	2.61	3.05	2.73	2.89
	g(*r*)	0.46	0.20	0.27	0.29
NTO/Poly-NIMMO	*r*/Å	3.05	3.09	2.63	2.85
	g(*r*)	0.42	0.38	0.39	0.40

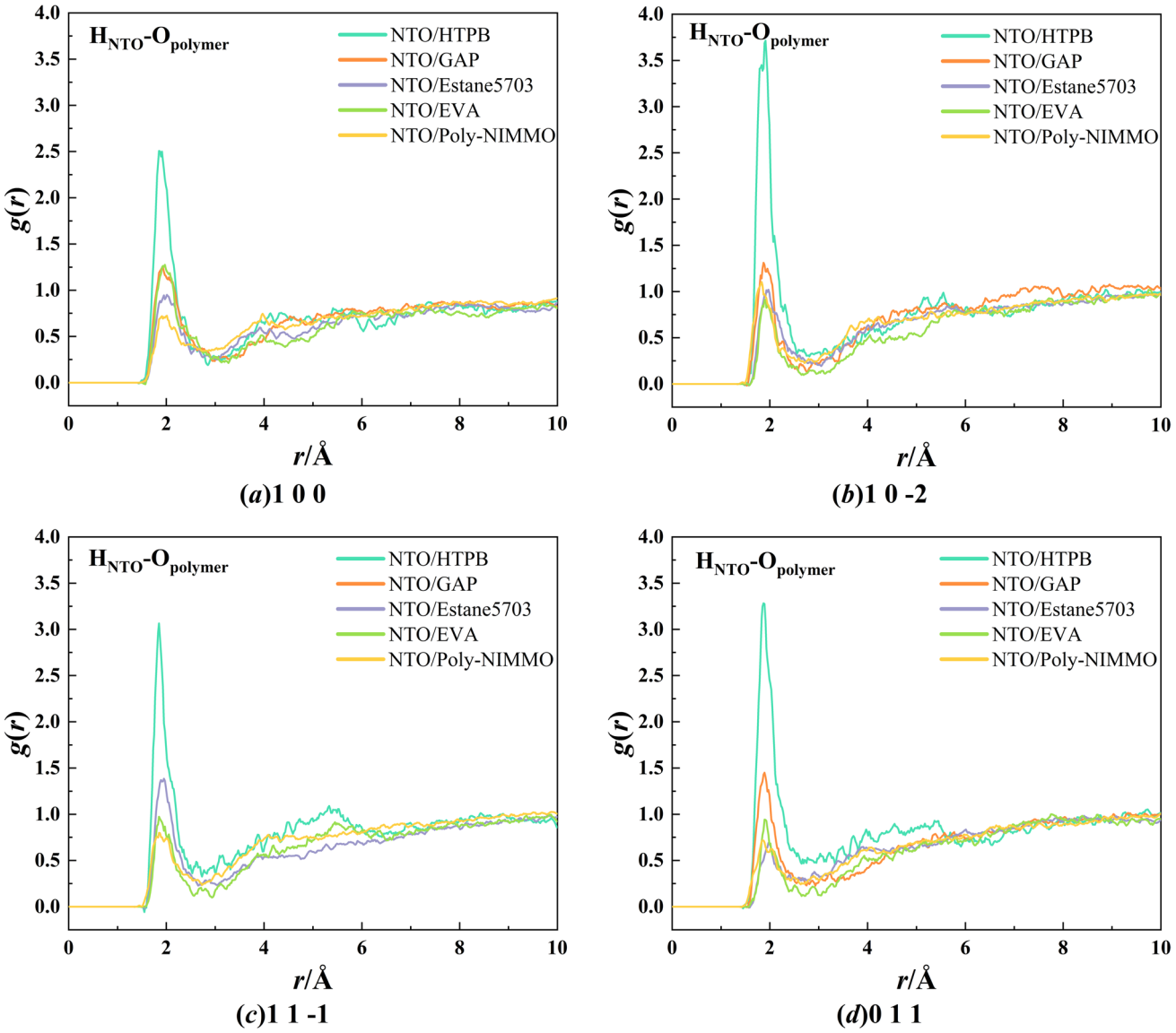

Fig. 6 The radial distribution function between H atoms of NTO and O atoms of polymers (HTPB, GAP, Estane5703, EVA, Poly-NIMMO)

interaction between them. Moreover, when the action distance is greater than 5.0 Å, there is a peak value, which indicates the existence of Coulomb's interaction.

The peak points and peak values of hydrogen bond interaction between the H atoms of NTO and O atoms of five binders are listed in Table 5, where the peak point corresponds to *r* at the maximum peak values. It can be concluded from Table 5 that the order of hydrogen bond interactions between the H atoms of NTO and O atoms of Estane5703 on different crystal faces is (1 0 0) > (1 1 − 1) > (0 1 1) > (1 0 − 2), which is consistent with the order of binding energy of different crystal faces. It shows that the interface interaction of NTO/Estane5703 composite system is mainly the hydrogen bond between the H atoms of NTO and the O atoms of Estane5703. Furthermore, for HTPB, EVA, and Poly-NIMMO, the strength of hydrogen bond interactions is basically consistent with the order of binding energy. Among them, the order of crystal faces with weak hydrogen bonding is slightly different from that of the above-mentioned binding energy, there exhibiting individual outliers. It is shown that the interaction strengths between the two crystal faces and the binders are approximated. This indicates that the interface interactions of NTO/HTPB, NTO/EVA, and NTO/Poly-NIMMO systems are mainly the hydrogen bond between the H atoms of NTO and the O atoms of HTPB, EVA, and Poly-NIMMO. However, the order of hydrogen bond interactions of NTO/GAP systems is (1 0 0) > (1 1 − 1) > (0 1 1) > (1 0 − 2). It can be found that the hydrogen bonds between NTO (1 0 − 2) crystal face and binder exhibit a visible difference compared with the binding energy. It shows that the hydrogen bond interactions of NTO/GAP systems may not be dominated by the hydrogen bond between the H atoms of NTO and the O atoms of GAP. In conclusion, the NTO (1 0 0) crystal face has the strongest hydrogen bond interaction in PBX systems, which is consistent with the comparison of binding energy. It can also be seen from Table 5 that the hydrogen bond interactions between the composite systems composed of GAP and different crystal faces of NTO are the strongest. And this result is also consistent with that of binding energy analysis.

Figure 7 shows the RDF between the H atoms of NTO and N atoms of three binders. It can be seen from Fig. 7 that for different crystal faces, $g(r)$ has a strong peak in the hydrogen bonding interval, which demonstrates that the interactions between the H atoms of NTO and the N atoms of the three binders are mainly hydrogen bonding, and there is a certain van der Waals interaction. Moreover, there is also a peak at the position where the action range is greater than 5.0 Å, which indicates that there is Coulomb's interaction in the systems.

Table 6 shows the peak points and peak values of hydrogen bond interaction between the H atoms of NTO and the N atoms of three binders. It can be found that, no matter which crystal face, the order of hydrogen bond interactions between the N atoms of the three binders and the H atoms of NTO is NTO/GAP > NTO/Poly-NIMMO > NTO/Estane5703. Compared with different crystal faces, the order of the hydrogen bond interactions of NTO/GAP systems is (1 0 0) > (1 0 − 2) > (0 1 1) > (1 1 − 1). Among which the hydrogen bond interactions between NTO (0 1 1) and NTO (1 1 − 1) crystal faces and GAP polymer are different from the binding energy, but the difference is minimal. The overall trend is consistent with the binding energy, which indicates that the interface interactions of NTO/GAP composite systems are mainly the hydrogen bond formed between the H atoms of NTO and the N atoms of GAP.

Cohesive energy density

Cohesive energy density (CED) is the energy required for 1 mol condensate per unit volume to overcome intermolecular interaction and become gaseous. In molecular dynamics simulation, CED is the sum of van der Waals' force and electrostatic force, that is, non-bonding interaction. In PBXs, CED can be defined as the total energy required to separate the binder and explosive molecules from each other, which reflects the strength of intermolecular interaction [37, 46]. The larger the CED value, the higher the energy required to change the explosives from condensed phase to gas phase, the more difficult it is to decompose and explode, and the better the safety of the system.

The CED calculation of trajectory files of NTO models and PBX interface models is carried out. Table 7 lists the calculated total values of CED and the specific values of its components van der Waals' force and electrostatic force. It can be seen from Table 7 that the cohesive energy density is equal to the sum of van der Waals' force and electrostatic force, and the contribution of electrostatic force to the cohesive energy density is greater than van der Waals' force, demonstrating that the intermolecular interactions in the systems are dominated by electrostatic force. This content is consistent with the results of the RDF analysis.

The results in Table 7 are compared and analyzed. It can be found that PBX systems containing GAP and Poly-NIMMO have good stability on the same crystal face. The values of CED of systems with Estane5703 added on (1 0 0), (1 0 − 2), and (1 1 − 1) crystal faces are the lowest. However, on the (0 1 1) crystal face, the value of CED of the system with Estane5703 is the largest. For the same polymers, except for the sequence of CED values of NTO/Estane5703 systems being (1 0 0) > (0 1 1) > (1 1 − 1) > (1 0 − 2), the sequence of PBX systems with other polymers is (1 0 0) > (1 1 − 1) > (0 1 1) > (1 0 − 2). There is little difference in CED values of NTO/Estane5703 systems on (1 1 − 1) and (0 1 1) crystal faces. The reason for this difference may be that the chain of Estane5703 is too long, and there are errors in the

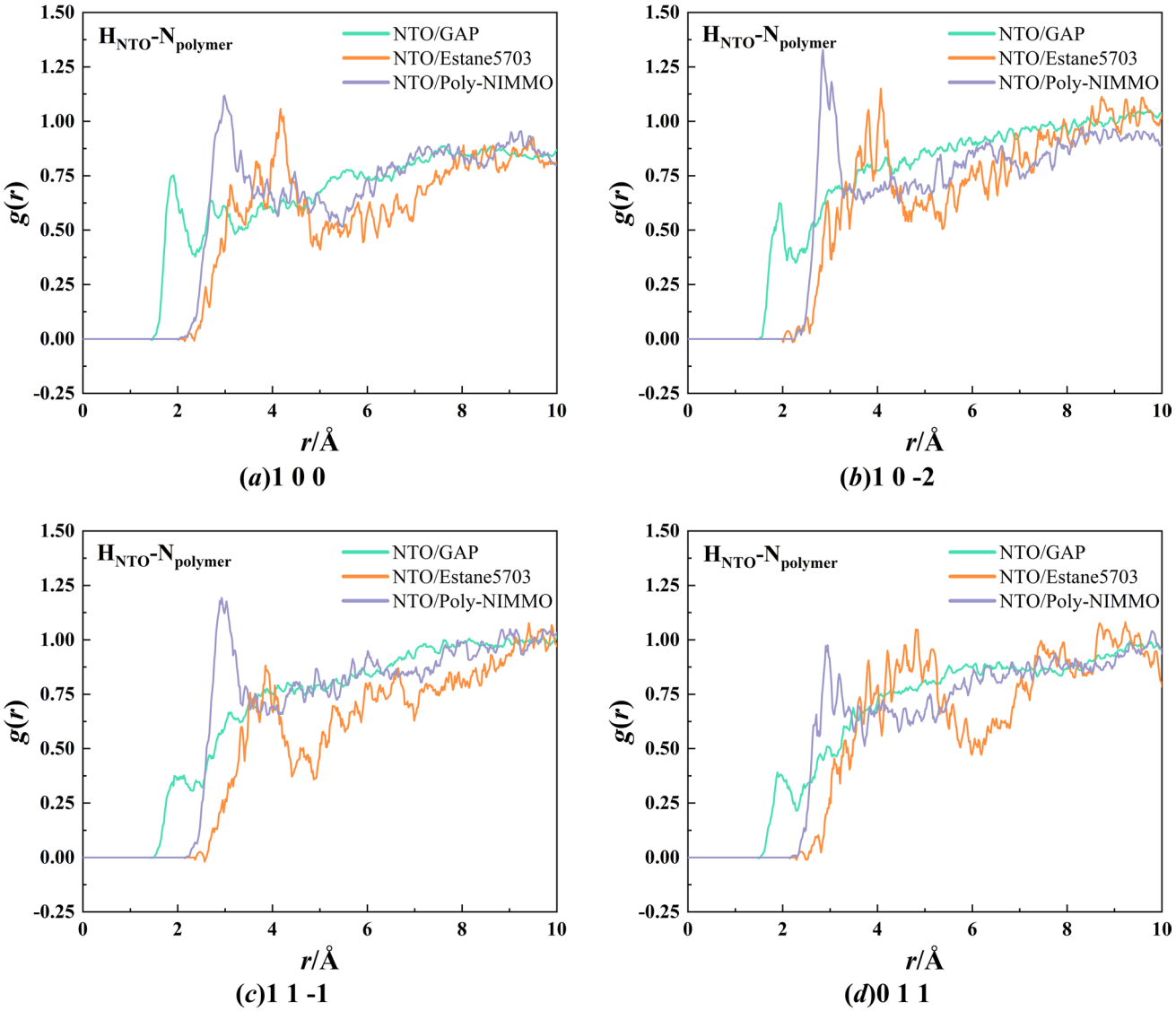

Fig. 7 The radial distribution function between H atoms of NTO and N atoms of polymers (GAP, Estane5703, Poly-NIMMO)

process of compression modeling close to theoretical density. On the whole, the composite systems combined with (1 0 0) face have low mechanical sensitivity and good safety, while the composite systems combined with (1 0 − 2) face have low safety.

Table 6 The peak points and peak values of hydrogen bond interaction between H atoms of NTO and N atoms of binders

Systems	Facet	1 0 0	1 0 − 2	1 1 − 1	0 1 1
NTO/GAP	*r*/Å	2.67	2.89	3.09	2.95
	g(*r*)	0.69	0.75	0.69	0.62
NTO/Estane5703	*r*/Å	3.07	2.91	3.07	3.07
	g(*r*)	0.79	0.84	0.63	0.55
NTO/Poly-NIMMO	*r*/Å	3.05	2.89	3.01	2.95
	g(*r*)	1.20	1.56	1.43	1.06

The weighted average values of the total value of CED and its components, van der Waals' force and electrostatic force, are calculated to characterize the magnitude of CED and its components of the whole structure of PBXs, as shown in Fig. 8. It can be seen from Fig. 8 that the order of cohesive energy density between different binders and NTO is NTO/GAP > NTO/Poly-NIMMO > NTO/HTPB > NTO/EVA > NTO/Estane5703. In addition, it can be seen that the CED values of PBX systems with binders are lower than that of pure NTO systems. Therefore, the NTO crystal is more difficult to vaporize than the NTO-based PBXs; that is, the NTO crystal is more stable. The reason for this phenomenon may be due to the high regularity of pure explosive crystals [37].

Table 7 The values of CED and CED distributions of NTO and NTO-based PBX systems

Systems	Facet	CED/J•cm^{-3}	vdW/J•cm^{-3}	Electrostatic/J•cm^{-3}
NTO	1 0 0	1473.0 ± 0.668	592.1 ± 0.514	881.4 ± 0.794
	1 0 − 2	1129.0 ± 0.446	492.0 ± 0.525	636.6 ± 0.609
	1 1 − 1	1282.0 ± 0.493	569.9 ± 0.452	712.3 ± 0.581
	0 1 1	1209.0 ± 0.481	524.8 ± 0.486	684.1 ± 0.607
NTO/HTPB	1 0 0	1345.0 ± 0.463	565.1 ± 0.599	779.9 ± 0.630
	1 0 − 2	964.5 ± 0.497	420.5 ± 0.410	544.0 ± 0.591
	1 1 − 1	1016.0 ± 0.489	443.6 ± 0.457	572.4 ± 0.655
	0 1 1	974.6 ± 0.416	425.9 ± 0.425	548.7 ± 0.546
NTO/GAP	1 0 0	1379.0 ± 0.533	576.6 ± 0.501	802.8 ± 0.612
	1 0 − 2	992.9 ± 0.402	428.1 ± 0.414	564.8 ± 0.584
	1 1 − 1	1052.0 ± 0.531	458.4 ± 0.431	593.4 ± 0.571
	0 1 1	1009.0 ± 0.445	432.5 ± 0.425	576.1 ± 0.545
NTO/Estane5703	1 0 0	1139.0 ± 0.586	359.8 ± 0.672	779.0 ± 0.615
	1 0 − 2	923.3 ± 0.453	403.9 ± 0.407	519.5 ± 0.589
	1 1 − 1	1012.0 ± 0.393	447.2 ± 0.455	565.1 ± 0.530
	0 1 1	1017.0 ± 0.406	451.3 ± 0.444	565.7 ± 0.499
NTO/EVA	1 0 0	1328.0 ± 0.496	555.0 ± 0.511	773.2 ± 0.616
	1 0 − 2	936.2 ± 0.405	411.1 ± 0.378	525.1 ± 0.501
	1 1 − 1	1039.0 ± 0.406	471.7 ± 0.420	567.3 ± 0.523
	0 1 1	969.7 ± 0.364	430.6 ± 0.432	539.1 ± 0.562
NTO/Poly-NIMMO	1 0 0	1382.0 ± 0.551	573.4 ± 0.631	808.9 ± 0.708
	1 0 − 2	978.9 ± 0.422	423.0 ± 0.365	555.9 ± 0.550
	1 1 − 1	1046.0 ± 0.413	455.6 ± 0.466	590.0 ± 0.547
	0 1 1	991.2 ± 0.445	427.8 ± 0.440	563.4 ± 0.590

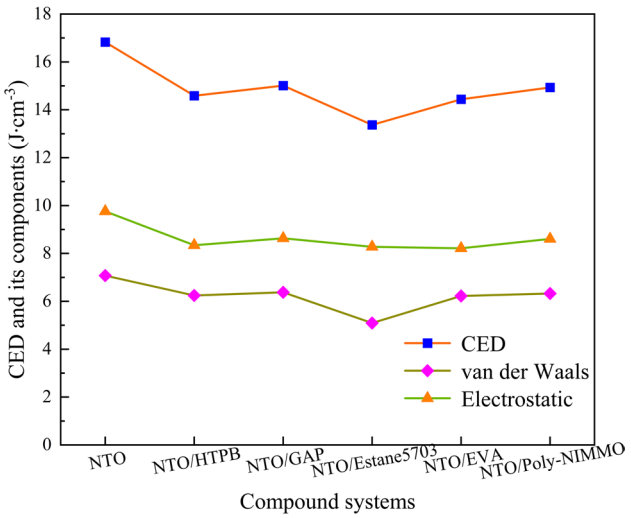

Fig. 8 The weighted average values of the total value of CED and its components of NTO and NTO-based PBXs

Although the addition of binders affects the original regularity of explosive molecules and leads to the decrease of CED, it does not mean to say that PBXs with binders are sensitive. Comparing the CED values of different systems under the same conditions can better correlate the level of sensitivity.

It can be seen from Fig. 8 that the trend of CED is basically consistent with its components. It can also be observed from Table 7 that the CED values and component values of different NTO-based PBXs on the same crystal face are basically the same, and the difference is very small, indicating that the statistical average of CED is not affected by the MD initial model. On the whole, the GAP/NTO system is the most stable of all PBX systems.

Mechanical properties

Mechanical properties play a very important role in the manufacture and application of energetic materials. Energetic materials are special functional materials, and their mechanical properties are fundamental properties in production, processing, and application. There is an internal relationship between the stress and strain of the material. At a certain temperature, the definite relationship between them reflects the inherent characteristics of the material. When the material can show its elasticity and the strain is small enough, the stress is proportional to the corresponding strain, following Hooke's law [47]. It can be described as:

$$\sigma_i = C_{ij}\varepsilon_j,\ i,j = 1,\cdots,6 \tag{6}$$

where C_{ij} is an elastic coefficient matrix with 36 elements. Because elastic deformation is a reversible process, the elastic matrix is symmetrical. For this reason, even the extremely anisotropic system has only 21 elastic coefficients.

According to the Reuss average method [48], the bulk modulus (K) and shear modulus (G) of the material after obtaining the elastic coefficient matrix can be calculated by the following equations:

$$K_R=\left[S_{11}+S_{22}+S_{33}+2\left(S_{12}+S_{23}+S_{31}\right)\right]^{-1} \tag{7}$$

$$G_R=15\left[4\left(S_{11}+S_{22}+S_{33}\right)-4\left(S_{12}+S_{23}+S_{31}\right)+3\left(S_{44}+S_{55}+S_{66}\right)\right]^{-1} \tag{8}$$

where subscript R represents the Reuss average. $S=\left[S_{ij}\right]$ is the flexibility coefficient matrix, which is equal to the inverse matrix of the elasticity coefficient matrix C; that is, $S=C^{-1}$. It is worth noting that even if the number of independent elastic coefficients is 21 in the most general case, the Reuss modulus is only related to nine compliance coefficients.

After the values of bulk modulus and shear modulus are obtained, the tensile modulus (E) and Poisson's ratio (γ) can be calculated according to the values of both bulk modulus and shear modulus by the following equation:

$$E=2G(1+\gamma)=3K(1-2\gamma) \tag{9}$$

And plastic fracture strength characteristics are related to the elasticity of materials. Therefore, researchers use the invariable elastic characteristic data to qualitatively predict the plasticity and fracture strength characteristics of materials [49]. Generally speaking, six mechanical parameters, namely bulk modulus (K), shear modulus (G), tensile modulus (E), Poisson's ratio (γ), Cauchy pressure (C_{12}-C_{44}), and the ratio of bulk modulus to shear modulus (K/G), are used as the evaluation criteria of mechanical properties [50]. Generally, the shear modulus (G) is related to the stiffness; that is, the greater its value, the greater its ability to prevent plastic deformation of materials. Tensile modulus (E) is a physical quantity used to describe the resistance of materials to elastic deformation, also known as Young's modulus. It is used to measure the rigidity of isotropic elastomer; that is, the greater the tensile modulus, the greater the rigidity of the material, and the smaller the elastic deformation of the material under a certain stress. The bulk modulus (K) is used to correlate the fracture strength of materials. The greater the value, the greater the fracture strength of the material. The ratio of bulk modulus to shear modulus (K/G) is used to predict the ductility of materials, and a larger value indicates that the ductility of materials is superior. In addition, Cauchy's pressure (C_{12}–C_{44}) can also predict the ductility of materials. If Cauchy's pressure is negative, the material is brittle; if it is positive, it demonstrates that the material has good ductility. Even though both values of K/G and Cauchy's pressure can judge the ductility of materials, the basis of their judgment is different. The difference is that the former is based on the degree of plastic deformation, while the latter is based on the fracture morphology. The above properties based on different crystal faces of pure NTO systems and NTO-based PBX systems are calculated and listed in Table 8. In the simulation process, the constant strain method is used as the calculation method, the number of strains is set to 4, and the maximum strain amplitude is set to 0.003. Among them, the units of bulk modulus, shear modulus, tensile modulus, and Cauchy's pressure are GPa.

It can be seen from Table 8 that compared with pure NTO systems, the engineering modulus of PBXs with binders, such as E, K, and G, are significantly reduced. This also means that the rigidity of PBXs is weaker, and the flexibility is stronger than that of the NTO crystal. In addition, Poisson's ratio γ and K/G of systems were increased by adding binders, which indicated that the ductility of systems was improved.

There is no doubt that the binder can basically improve the mechanical properties of the system regardless of different crystal faces or various binders. By comparing the bulk modulus, shear modulus, and tensile modulus of different crystal faces, it can be concluded that the mechanical properties of systems are improved more or less when various binders are placed in (1 0 0), (1 0 − 2), and (1 1 − 1) crystal faces. Moreover, EVA is the best binder to improve the performance of these three crystal faces. For instance, the tensile modulus of the (1 0 − 2) crystal face of the pure NTO system reaches 17.59 GPa, which demonstrates that its rigidity is strong. When a small amount of EVA is placed on the NTO (1 0 − 2) surface, the tensile modulus of the system decreases to 4.63 GPa, which means that the flexibility of this PBX is greatly improved. For the NTO (0 1 1) crystal face, HTPB might have no obvious effect on ameliorating the ability of shear resistance and tensile resistance of the systems. Compared with Poisson's ratio, it can be observed that Poisson's ratio of all PBX systems is around 0.3–0.4, which indicates that all systems are plastic. Compared with the pure NTO systems, the plasticity of the systems in which the binders are placed on the NTO (1 0 − 2) and NTO (1 1 − 1) crystal faces are improved. But for NTO (1 0 0) and NTO (0 1 1) crystal faces, EVA may have little effect on improving the plasticity of the systems. For the four crystal faces, Estane5703 can improve the plasticity of the system well and stably. In addition, it can be observed that the values of K/G of different crystal faces are consistent with the contrast trend of Poisson's ratio. This means that the PBX systems containing Estane5703 have excellent formability. The K/G values of different systems are distinct from the trend of Cauchy's pressure, which just vindicates that although both of them are used to judge the ductility of materials, the judgment basis is different.

Table 8 Mechanical properties of NTO and NTO-based PBXs

Systems	Facet	*K*	*G*	*E*	*γ*	*K/G*	Cauchy's pressure (C_{12}–C_{44})
NTO	1 0 0	7.16	3.15	8.25	0.31	−1.77	2.27
	1 0 −2	8.68	7.57	17.59	0.16	3.71	1.15
	1 1 −1	7.09	2.95	7.77	0.32	−0.80	2.41
	0 1 1	5.57	2.01	5.37	0.34	1.32	2.78
NTO/HTPB	1 0 0	5.42	2.29	6.01	0.32	−1.30	2.37
	1 0 −2	4.93	1.90	5.06	0.33	1.64	2.59
	1 1 −1	5.28	2.12	5.61	0.32	1.55	2.49
	0 1 1	5.49	2.07	5.52	0.33	1.44	2.65
NTO/GAP	1 0 0	4.74	2.25	5.83	0.29	−1.55	2.10
	1 0 −2	5.25	2.04	5.42	0.33	1.30	2.57
	1 1 −1	4.49	0.79	2.25	0.42	0.32	5.66
	0 1 1	4.85	1.66	4.48	0.35	1.72	2.91
NTO/Estane5703	1 0 0	5.74	2.30	6.08	0.32	−0.53	2.50
	1 0 −2	5.51	2.06	5.50	0.33	1.64	2.67
	1 1 −1	5.39	1.91	5.12	0.34	1.44	2.82
	0 1 1	5.04	1.68	4.55	0.35	1.81	2.99
NTO/EVA	1 0 0	4.01	1.99	5.13	0.29	−2.06	2.01
	1 0 −2	4.92	1.72	4.63	0.34	1.30	2.85
	1 1 −1	5.08	0.69	1.99	0.43	1.67	7.33
	0 1 1	4.77	1.91	5.06	0.32	1.17	2.50
NTO/Poly-NIMMO	1 0 0	5.89	2.04	5.49	0.34	−0.55	2.88
	1 0 −2	5.73	2.21	5.89	0.33	1.52	2.59
	1 1 −1	4.80	1.92	5.09	0.32	1.84	2.49
	0 1 1	4.87	1.59	4.30	0.35	0.44	3.07

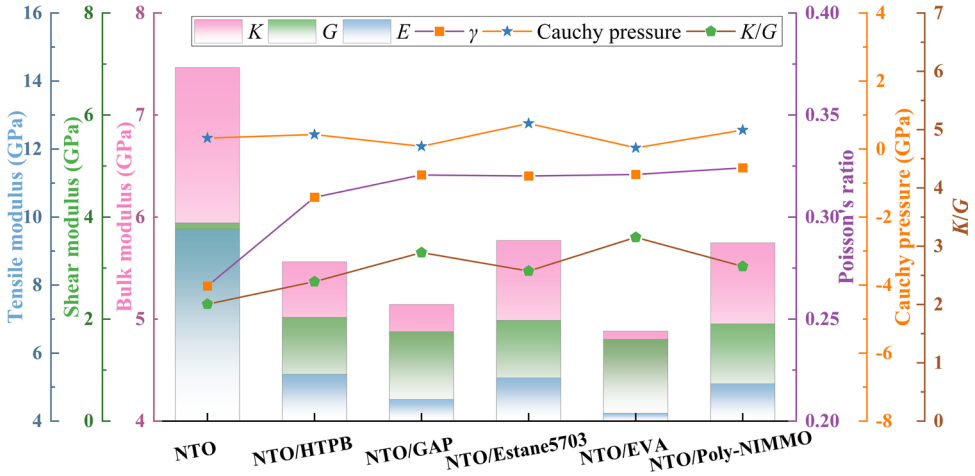

Fig. 9 The weighted average mechanical properties of NTO and NTO-based PBXs

In addition, the weighted averages of mechanical properties were calculated to characterize and analyze the mechanical properties of the whole composite system structure of PBXs, as shown in Fig. 9. It can be clearly seen from the figure that the shear modulus (*G*), bulk modulus (*K*), and tensile modulus (*E*) of PBXs are lower than those of pure NTO systems. This shows that the stiffness, fracture strength, and tensile strength of NTO-based PBXs are significantly reduced by adding binders. This phenomenon is consistent with the fact that adding binders can improve the plasticity of PBXs. Furthermore, the order of plasticity is NTO/EVA > NTO/GAP > NTO/Poly-NIMMO > NTO/Estane5703 > NTO/HTPB. Comparing Poisson's ratio (*γ*) of different systems, the values of Poisson's ratio of each

NTO-based PBXs are very close. The order of Poisson's ratio of PBX systems is NTO/Poly-NIMMO > NTO/EVA > NTO/GAP > NTO/Estane5703 > NTO/HTPB > NTO. Generally speaking, materials with Poisson's ratio between 0.2 and 0.4 are considered plastic. Therefore, both NTO and NTO-based PBX systems have plasticity, and the addition of binders improves the plasticity of systems. We compare the ratio of bulk modulus to shear modulus to judge the toughness of the system. It can be clearly seen from Fig. 9 that compared with pure NTO systems, the *K/G* values of PBX systems are obviously increased. This indicates that the toughness of PBX systems is better than that of pure NTO systems. And its toughness is NTO/EVA > NTO/GAP > NTO/Poly-NIMMO > NTO/Estane5703 > NTO/HTPB > NTO. In addition, the Cauchy pressure of different systems is compared to analyze the ductility. It can be seen that the Cauchy pressure values of all systems are positive, demonstrating that all systems have certain ductility. However, comparing the magnitude of its value, NTO/Estane5703 > NTO/Poly-NIMMO > NTO/HTPB > NTO/GAP > NTO/EVA, it can be found that the addition of Estane5703, Poly-NIMMO, and HTPB may enhance the ductility of the systems, which is beneficial to processing, molding, and application. However, the addition of GAP and EVA binders may reduce the formability of the systems.

Conclusions

Molecular dynamics simulations have been conducted for NTO models and NTO/HTPB, NTO/EVA, NTO/GAP, NTO/Poly-NIMMO, and NTO/Estane5703 interface models; it can be concluded as follows:

1. Comparing the unit binding energy of different systems, it can be found that the polymer binder has a high probability to interact with the (1 0 0) crystal face of NTO no matter which binder. Furthermore, the PBX systems composed of GAP and NTO is the most stable of all established systems. The comprehensive analysis demonstrates that the order of compatibility is NTO/GAP > NTO/Estane5703 > NTO/HTPB > NTO/Poly-NIMMO > NTO/EVA.
2. The RDF analysis indicates that the interface interactions of different systems are mainly hydrogen bonds. Furthermore, it can be found that the hydrogen bond is between the H atoms of NTO and the O atoms of Estane5703, HTPB, EVA, and Poly-NIMMO or the N atoms of GAP. The RDF analysis also verified that the NTO (1 0 0) crystal face has the strongest hydrogen bond interaction and the NTO-based PBXs with GAP binder have the best hydrogen bond interaction.
3. The CED analysis demonstrates that the contribution of electrostatic force to cohesive energy density is greater than van der Waals' force. The comprehensive analysis shows that the safety of PBXs is NTO/GAP > NTO/Poly-NIMMO > NTO/HTPB > NTO/EVA > NTO/Estane5703. On the whole, the composite systems combined with NTO (1 0 0) face have low mechanical sensitivity and good safety.
4. The rigidity, stiffness, and plasticity of PBX systems composed of different binders placed on (1 0 − 2) and (1 1 − 1) crystal faces are obviously improved. Considering the overall mechanical properties of PBX systems, the rigidity and stiffness, plasticity, and toughness of PBX systems with EVA, GAP, and Poly-NIMMO are all improved. The addition of Estane5703, Poly-NIMMO, and HTPB is beneficial to the improvement of the ductility of PBX systems.

Author Contribution Ying Huang and Ruijun Gou conceived and designed the study. Ying Huang and Xiaofeng Yuan performed simulation calculations. Ying Huang wrote the paper. Ruijun Gou, Yahong Chen, and Shuhai Zhang reviewed and edited the manuscript. All authors read and approved the manuscript.

Data Availability The datasets generated during and/or analyzed during the current study are available from the corresponding author on reasonable request.

Declarations

Competing Interests The authors declare no competing interests.

References

1. Badgujar DM, Talawar MB, Asthana SN, Mahulikar PP (2008) Advances in science and technology of modern energetic materials: an overview. J Hazard Mater 151(2–3):289–305. https://doi.org/10.1016/j.jhazmat.2007.10.039
2. Baytos JF (1980) LASL explosive property data. University of California Press
3. Mathieu J, Stucki H (2004) Military high explosives. CHIMIA 58(6):383–389. https://doi.org/10.2533/000942904777677669
4. Dong HS, Zhou FF (1984) High energy explosives and correlative physical properties. Science Press, Beijing
5. Li MM, Shen RQ, Li FS (2011) Molecular dynamics simulation of binding energies, mechanical properties and energetic performance of the RDX/BAMO propellant. Acta Phys-Chim Sin 27(6):1379–1385. https://doi.org/10.3866/PKU.WHXB20110601
6. Song XY, Xing XL, Zhao SX, Ju XH (2019) Molecular dynamics simulation on TKX-50/fluoropolymer. Modell Simul Mater Sci Eng 28(1):015004. https://doi.org/10.1088/1361-651X/ab5497
7. Lan GC, Jin SH, Wang DX, Li J, Lu ZY, Jing BC, Li LJ (2018) Investigation of the effect of the CAB/A3 system on HNIW-based PBXs using molecular dynamics. J Mol Model 24(7):1–9. https://doi.org/10.1007/s00894-018-3670-3

8. Li SS, Xiao JJ (2021) Molecular dynamics simulations for effects of fluoropolymer binder content in CL-20/TNT based polymer-bonded explosives. Molecules 26(16):4876. https://doi.org/10.3390/molecules26164876
9. Wang XJ, Xiao JJ (2017) Molecular dynamics simulation studies of the ε-CL-20/HMX co-crystal-based PBXs with HTPB. Struct Chem 28(6):1645–1651. https://doi.org/10.1007/s11224-017-0930-2
10. Xiao HM, Li JS, Dong HS (2001) A quantum-chemical study of PBX: intermolecular interactions of TATB with CH2F2 and with linear fluorine-containing polymers. J Phys Org Chem 14(9):644–649. https://doi.org/10.1002/poc.403.abs
11. Xiao JJ, Fang GY, Ji GF, Xiao HM (2005) Simulation investigations in the binding energy and mechanical properties of HMX-based polymer-bonded explosives. Chin Sci Bull 50(1):21–26. https://doi.org/10.1360/982004-147
12. Xiao JJ, Huang YC, Hu YJ, Xiao HM (2005) Molecular dynamics simulation of mechanical properties of TATB/fluorine-polymer PBXs along different surfaces. Sci China, Ser B: Chem 48(6):504–510. https://doi.org/10.1360/042004-61
13. Lu YY, Shu YJ, Liu N, Lu XM, Xu MH (2018) Molecular dynamics simulations on ε-CL-20-based PBXs with added GAP and its derivative polymers. RSC Adv 8(9):4955–4962. https://doi.org/10.1039/c7ra13517c
14. Xu XJ, Xiao JJ, Huang H, Li JS, Xiao HM (2007) Molecular dynamics simulations on the structures and properties of ε-CL-20-based PBXs. Sci China, Ser B: Chem 50(6):737–745. https://doi.org/10.1007/s11426-007-0141-6
15. Zhang M, Li C, Gao HQ, Fu W, Li YY, Tang LW, Zhou ZM (2016) Promising hydrazinium 3-nitro-1, 2, 4-triazol-5-one and its analogs. J Mater Sci 51(24):10849–10862. https://doi.org/10.1007/s10853-016-0296-7
16. Singh G, Kapoor IPS, Tiwari SK, Felix PS (2001) Studies on energetic compounds: part 16. chemistry and decomposition mechanisms of 5-nitro-2, 4-dihydro-3H-1, 2, 4-triazole-3-one (NTO). J Hazard Mater 81(1–2):67–82. https://doi.org/10.1016/S0304-3894(00)00289-2
17. Becuwe A, Delclos A (1993) Low-sensitivity explosive compounds for low vulnerability warheads. Propellants, Explos, Pyrotech 18(1):1–10. https://doi.org/10.1002/prep.19930180102
18. Trzciński WA (2020) Study of shock initiation of an NTO-based melt-cast insensitive composition. Propellants, Explos, Pyrotech 45(9):1472–1477. https://doi.org/10.1002/prep.202000050
19. Viswanath DS, Ghosh TK, Boddu VM (2018) 5-Nitro-2, 4-dihydro-3H-1, 2, 4-triazole-3-one (NTO). In: Emerging energetic materials: synthesis, physicochemical, and detonation properties. Springer, Dordrecht 163–211. https://doi.org/10.1007/978-94-024-1201-7_5
20. Smith MW, Cliff MD (1999) NTO-based explosive formulations: a technology review.
21. Zhou WJ, Ma YN, Wang KY, Wang M, Zhang G, Shao YH (2010) Interfacial interaction between NTO and bindings. Chin J Explos Propellants 33(4):40–43. https://doi.org/10.14077/j.issn.1007-7812.2010.04.010
22. Hang GY, Yu WL, Wang T, Wang JT, Miao S (2019) Molecular dynamics investigation on crystal defect of HMX/NTO cocrystal explosive. Acta Armamentarii 40(1):49. https://doi.org/10.3969/j.issn.1000-1093.2019.01.007
23. Du LXS, Jin SH, Shu QH, Li LJ, Chen K, Chen ML, Wang JF (2022) The investigation of NTO/HMX-based plastic-bonded explosives and its safety performance. Def Technol 18(1):72–80. https://doi.org/10.1016/j.dt.2021.04.002
24. Yan QL, Zeman S, Elbeih A (2012) Recent advances in thermal analysis and stability evaluation of insensitive plastic bonded explosives (PBXs). Thermochim Acta 537:1–12. https://doi.org/10.1016/j.tca.2012.03.009
25. Jaidann M, Lussier LS, Bouamoul A, Abou-Rachid H, Brisson J (2009) Effects of interface interactions on mechanical properties in RDX-based PBXs HTPB-DOA: molecular dynamics simulations. In: International conference on computational science. Springer, Berlin, Heidelberg, 131–140. https://doi.org/10.1007/978-3-642-01973-9_15.
26. Brochu D, Abou-Rachid H, Soldera A, Brisson J (2017) Sensitivity of polymer-bonded explosives from molecular modeling data. Int J Energ Mater Chem Propul 16(4). https://doi.org/10.1615/IntJEnergeticMaterialsChemProp.2018021264.
27. Xiao JJ, Ma XF, Zhu W, Huang YC, Xiao HM, Huang H, Li JS (2007) Molecular dynamics simulations of polymer-bonded explosives (PBXs): modeling, mechanical properties and their dependence on temperatures and concentrations of binders. Propellants, Explos, Pyrotech 32(5):355–359. https://doi.org/10.1002/prep.200700039
28. Xiao JJ, Wang WR, Chen J, Ji GF, Zhu W, Xiao HM (2012) Study on the relations of sensitivity with energy properties for HMX and HMX-based PBXs by molecular dynamics simulation. Phys B (Amsterdam, Neth) 407(17):3504–3509. https://doi.org/10.1016/j.physb.2012.05.010
29. Zhu W, Wang XJ, Xiao JJ, Zhu WH, Sun H, Xiao HM (2009) Molecular dynamics simulations of AP/HMX composite with a modified force field. J Hazard Mater 167(1–3):810–816. https://doi.org/10.1016/j.jhazmat.2009.01.052
30. Sun H (1998) COMPASS: an ab initio force-field optimized for condensed-phase applications overview with details on alkane and benzene compounds. J Phys Chem B 102(38):7338–7364. https://doi.org/10.1021/jp980939v
31. Hang GY, Yu WL, Wang T, Wang JT, Li Z (2018) Theoretical investigations on stabilities, sensitivity, energetic performance and mechanical properties of CL-20/NTO cocrystal explosives by molecular dynamics simulation. Theor Chem Acc 137(8):1–14. https://doi.org/10.1007/s00214-018-2297-x
32. Wang JY, Jin SH, Chen SS, Li LJ, Wang DX, Lu ZY, Wang N, Wang JF (2018) Molecular dynamic simulations for FOX-7 and FOX-7 based PBXs. J Mol Model 24(7):1–9. https://doi.org/10.1007/s00894-018-3687-7
33. Yu YH, Chen SS, Li X, Zhu JP, Liang H, Zhang XX, Shu QH (2016) Molecular dynamics simulations for 5, 5′-bistetrazole-1, 1′-diolate (TKX-50) and its PBXs. RSC Adv 6(24):20034–20041. https://doi.org/10.1039/c5ra27912g
34. Zhao Y, Xie WX, Qi XF, Liu YF, Tang QF, Song KG, Zhang W (2019) Comparison of the interfacial bonding interaction between GAP matrix and ionic/non-ionic explosive: computation simulation and experimental study. Appl Surf Sci 497:143813. https://doi.org/10.1016/j.apsusc.2019.143813
35. Li JZ, Fan XZ, Zhang GF, Yu HJ, Tang QF, Fu XL (2016) Hardener systems of energetic binder PolyNIMMO. Acta Armamentarii 37(8):1401. https://doi.org/10.3969/j.issn.1000-1093.2016.08.009
36. Fu JB, Wang BG, Chen YF, Li YC, Tan X, Wang BY, Ye BY (2021) Computational analysis the relationships of energy and mechanical properties with sensitivity for FOX-7 based PBXs via MD simulation. R Soc Open Sci 8(2):200345. https://doi.org/10.1098/rsos.200345
37. Li J, Jin SH, Lan GC, Chen K, Liu W, Zhang XP, Chen SS, Li LJ (2020) A molecular dynamics study and detonation parameters calculation of 5, 5'-dinitramino-3, 3'-bi [1, 2, 4-triazolate] carbohydrazide salt (CBNT) and its PBXs. J Energ Mater 38(3):283–294. https://doi.org/10.1080/07370652.2019.1684595
38. Zhurova EA, Pinkerton AA (2001) Chemical bonding in energetic materials: β-NTO. Acta Crystallogr, Sect B: Struct Sci 57(3):359–365. https://doi.org/10.1107/S0108768100020048
39. Trzciński W, Belaada A (2016) 1, 1-Diamino-2, 2-dinitroethene (DADNE, FOX-7)–Properties and formulations (a review). Cent Eur J Energ Mater 13(2):527-544. https://doi.org/10.22211/cejem/65000

40. Andersen HC (1980) Molecular dynamics simulations at constant pressure and/or temperature. J Chem Phys 72(4):2384–2393. https://doi.org/10.1063/1.439486
41. Karasawa N, III Goddard WA (2002) Force fields, structures, and properties of poly (vinylidene fluoride) crystals. Macromolecules 25(26):7268–7281. https://doi.org/10.1021/ma00052a031
42. Martyna GJ, Tobias DJ, Klein ML (1994) Constant pressure molecular dynamics algorithms. J Chem Phys 101(5):4177–4189. https://doi.org/10.1063/1.467468
43. Li J, Jin SH, Lan GC, Ma X, Ruan J, Zhang B, Chen SS, Li LJ (2018) Morphology control of 3-nitro-1, 2, 4-triazole-5-one (NTO) by molecular dynamics simulation. Cryst Eng Comm 20(40):6252–6260. https://doi.org/10.1039/c8ce00756j
44. Brostow W (1977) Radial distribution function peaks and coordination numbers in liquids and in amorphous solids. Chem Phys Lett 49(2):285–288. https://doi.org/10.1016/0009-2614(77)80588-5
45. Hu WJ, Gou RJ, Zhang SH, Liu Y, Shang FQ, Chen YH, Bai H (2022) Theoretical investigation on the intermolecular interactions between 3-nitro-1, 2, 4-triazol-5-one and 2, 6-diamino-3, 5-dinitropyrazine-1-oxide using DFT methods. Chem Pap 76(5):2747–2758. https://doi.org/10.1007/s11696-021-02059-y
46. Hang GY, Yu WL, Wang T, Wang JT (2019) Theoretical investigations on structures, stability, energetic performance, sensitivity, and mechanical properties of CL-20/TNT/HMX cocrystal explosives by molecular dynamics simulation. J Mol Model 25(1):1–15. https://doi.org/10.1007/s00894-018-3887-1
47. Rice JR (1972) Elastic-plastic fracture mechanics. Brown University, Providence, RI Division of Engineering. https://doi.org/10.2172/4620799
48. Watt JP, Davies GF, O'Connell RJ (1976) The elastic properties of composite materials. Rev Geophys 14(4):541–563. https://doi.org/10.1029/RG014i004p00541
49. XCII Pugh SF (1954) Relations between the elastic moduli and the plastic properties of polycrystalline pure metals. Lond Edinb Dubl Phil Mag 45(367):823–843. https://doi.org/10.1080/14786440808520496
50. Xiao JJ, Zhu WH, Zhu W, Xiao HM (2013) Molecular dynamics simulation of high energy materials. Science Press, Beijing, pp 54–66